Numerical Investigation of the Effect of Muffler Geometry on Engine Performance

S. E. Ibitoye, [*] *I. k. Adegun, Y. Sanni*
Faculty of Engineering and Technology,
Department of Mechanical Engineering, University of Ilorin,
PMB 1515, Ilorin, Nigeria
[*]*ibiyoyeesegun@gmail.com*

ABSTRACT

Muffler is a part of an exhaust system fitted to IC engines for damping noise and to convey hot gases from the combustion chamber. Several research efforts have been put into the study of muffler. This is due to their significant effects on noise reduction, fuel consumption, efficiency and life span of engine. Good muffler minimizes noise, back pressure and engine fuel consumption. Currently, the price of petroleum products in the global market is high and very unstable. Therefore, conservation of fuel is very important, particularly to the end user. This study seeks to examine the effects of baffle holes on the fluid flow characteristics and forces on the baffle walls. Three muffler models were designed using Autodesk Investor 2015. ANSYS 16.0 was used as the CFD working tools to predict the flow characteristics and forces on the walls. Samples A, B and C were modeled to have 7, 13 and 26 holes, respectively while the diameter of the holes for samples A, B and C were 50, 37.5 and 25 mm, respectively. Navier-Stokes and energy transport equations govern the three muffler models. Muffler sample A displayed the lowest backpressure of 20.235 Pa, average wall temperature of 986.311 K and best fuel efficiency characteristics. Sample B had the lowest forces on the wall while Muffler C has the least advantage when compared with other models. Muffler sample B gave the optimum design characteristic considering fuel consumption engine efficiency and muffler durability.

Keywords*: Muffler; Backpressure; Wall Temperature; Exhaust Pipe; Baffle Holes*

ISSN 1823-5514, eISSN 2550-164X
Received for review: 2020-11-24
Accepted for publication: 2021-08-04
Published: 2022-01-15

Nomenclature

h	Heat transfer coefficient
k	Thermal conductivity
Nu	Nusselt number
P	Pressure
q	Heat transfer
r	Radius of the Tube
Re	Reynolds number
T	Temperature
U_r	Velocity along radial direction
$U_\emptyset$	Velocity along azimuthal direction
U_x	Velocity along axial direction
ρ	Density
μ	Dynamic viscosity
C_p	Specific heat capacity
D_h	Hydraulic diameter
U_{avg}	Average velocity
$\boldsymbol{\alpha}$	Thermal diffusivity
V_m	Muffler volume
S_w	Swept volume
n	Number of cylinder
D	Bore diameter
L	Stroke diameter

Introduction

Several investigations and findings have been carried to improve the product of automotive industry. Many of this research were focused around improving aesthetics and engine performance [1]–[3]. Automobiles are made of several component such as body, electrical and electronics systems, power-train and chassis among others [4]–[8]. Power-train and chassis consist of electrical powertrain component, braking system, engine component, cooling system, lubrication system, fuel system, steering system, transmission system suspension system and exhaust system [9]–[13]. Exhaust system is designed to convey the emission from the engine away from the driver and passengers and to reduce the emissions the vehicle releases into the environment [14], [15]. It control the delivery of hot gasses and provide information to the vehicle's computer in order to significantly improve vehicle performance and reduce the amount of noise generated by the vehicle. The major components of the exhaust system include exhaust manifold, catalytic converter, exhaust pipe, resonator, muffler, oxygen sensors and tailpipe [12], [15], [16].

Muffler is fitted to internal combustion engine for damping the noise and to convey hot gases from the combustion chamber [17]–[19]. Its main components includes inlet and outlet pipes, baffle plate or perforated pipe and chamber where the propagation of sound wave, pressure drop, temperature and velocity profile can be examined. A good muffler minimizes the back pressure which is the pressure that opposes the desired flow of fluid in a confined place and maximizes noise reduction.

Mufflers are classified as reactive, dissipative or combined muffler [20]–[21]. Reactive muffler reflects the sound waves back towards the source and prevent it from being transmitted along the pipe [22]. Therefore, more pressure will be built up due to the baffle. Dissipative muffler uses sound absorbing materials to reduce the acoustic power and convert it to heat energy, this created less pressure drop, while the combined muffler contain both reactive and absorptive materials to extend the noise attenuation performance over a wider noise spectrum [23].

Mufflers are designed and constructed in different geometrics. One of the most popular geometric is circular or spherical shape with an inlet and outlet pipes. some circular geometrics are with partitions to help reduce noise and back pressure. The design parameters mostly include: number of chambers, number of inlet and outlet pipes, diameter of inlet and outlet pipe, holes on the pipe or baffle, size and materials of muffler [24]–[26]. Other criteria for selecting a good muffler include transmission loss and insertion loss. Transmission loss is a measure of the difference between the acoustic power of the exhaust gas at the inlet and the outlet while Insertion loss is defined as the difference between acoustic power of the exhaust gas with muffler and without muffler. The noise reduction inside a muffler automatically generate back pressure due to restriction in the flow within the muffler chamber. The back pressure created by the muffler affect the efficiency of the engine, though, they are usually overcome by the power generated from the engine [25]. Therefore, there is a need to design a muffler that produces lesser back pressure which is often caused by obstruction or restriction with a tolerable noise.

Several research efforts have been put into the design and construction of muffler. Teja and Reddy investigated the back pressure in exhaust silencer of single cylinder diesel engine [27]. Comprehensive study on four different models of exhaust silencer was carried out and acusolve CFD for virtual simulation of back pressure was applied. Finite Element model of the silencer structure was generated using hyper mesh as the pre- processor and internal tube with fine holes were considered. It was reported that samples design 1, 2, 3, and 4 generated a total pressures drop of 4.45, 4.85, 4.58 and 4.64 kPa, respectively. It was concluded that silencer design 1, give a very low pressure drop and easy to manufacture. Kore *et al.* worked on performance evaluation of a reactive muffler using CFD [23]. GAMBIT was used to create mesh surface and defined boundary condition which was read and analyzed using

FLUENT. The simulated result indicated that the airflow in the expansion zone creates stagnation pressure that contributed to the back pressure of the silencer. Chaudhri *et al.*, after studying different types of silencers and design methods, it was concluded that the combined type of silencer was more efficient in noise reduction than reactive and absorptive silencer [28]. Ramganesh and Devaradjane analyzed the simulation of flow and prediction of back pressure of the silencer using CFD. ANSYS was used for the simulation and prediction of the exhaust back pressure [29]. They concluded that the back pressure of any silencer depends on the pipe in the expansion chamber.

Due to instability in the prices of petroleum products in the global market and need to minimize environmental pollution such as noise and greenhouse emission generated by IC engine [30], this study seeks to examine the effects of baffle holes on the fluid flow characteristics and forces on the baffle walls. These affect the fuel consumption and noise generated by the engine as well as muffler durability. The results of this study found application in the design of muffler for motorcycles, vehicles and generator sets. This is expected to reduce the noise generated by IC engines, minimize both backpressure and forces on the walls, reduce fuel consumption and improve the performance of the IC engines.

Methodology

In this section, the methods and techniques used were enumerated and discussed fully. The muffler samples were drawn with Autodesk Inventor Professional 2015 and imported into ANSYS 16.0 workbench for numerical analysis. Figures 1 (a), (b) and (c) show the isometric drawing of samples A, B and C, respectively while Figure 1(d) shows the typical Meshed sample. Samples A, B and C were modeled to have 7, 13 and 26 holes, respectively while the diameter of the holes for samples A, B and C were 50, 37.5 and 25 mm, respectively. The perforated areas of baffle plates were 40.4, 42.5 and 37.8% for samples A, B and C, respectively

Design parameters

According to Krunal *et al.*, several parameters were considered in other to achieve a good muffler design [31]. These include acoustic, geometric, economic, mechanical and back pressure.

Specifications of the selected diesel engine

The following engine parameters were considered in designing the muffler for diesel engine generator set (Ford product) [32]:

Bore diameter (D)	80 mm
Stroke length (L)	98 mm
Number of Cylinders	6

Engine power (P)	65hp
Maximum revolution per minute	1800
Transmission loss	30 DB
Allowable back pressure	10 inches of H_2o

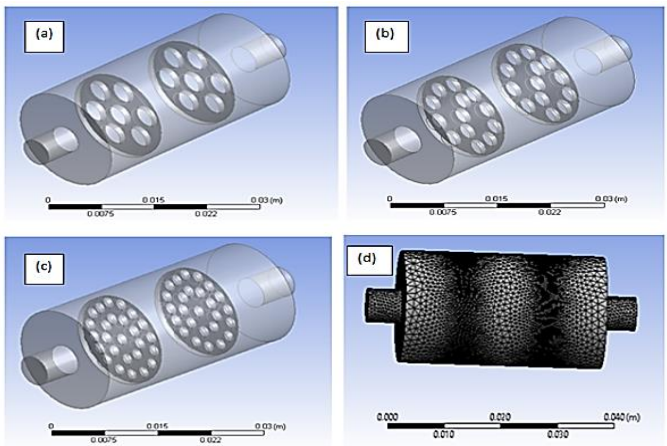

Figure 1: Isometric projection of muffler (a) sample A (7 holes), (b) sample B (13 holes), (c) sample C (26 holes), and (d) typical modeled sample.

Volume of muffler shell

$$\text{Volume of Muffler } V_m = S_w \times V_f \tag{1}$$

$$\text{Swept volume } S_w = \frac{\pi}{4}(D^2 L) \times \frac{n}{2} \tag{2}$$

where V_m is the volume of muffler, D is the bore diameter, L is the stroke diameter, n is the number of cylinders and S_w is the swept volume. Nasiruddin *et al.* reported that volume of muffler should be at least 12 to 25 times swept volume depending on space limits [32].

V_f = 18.5 were adopted. Therefore, $V_m = S_w \times 18.5 = 0.0273\ \text{m}^3$.

Muffler shell diameter

Consider a muffler of length L 800 mm; the muffler shell diameter is given Equation (3):

$$\text{d} = \sqrt{\left[\frac{V_m \times 4}{\pi L}\right]} = 0.208\ \text{m} \tag{3}$$

Diameter of exhaust pipe

The design of muffler diameter was obtained from Table 1, the standard grades for muffler design. Insertion loss is measured in A-weighted decibel (dBA). The 'body diameter of muffler ratio exhaust pipe' and 'length of muffler ratio exhaust pipe' are dimensionless parameters used for the calculation of the muffler length and body diameter in the design of muffler [33]. These parameters are stipulated by America Society of Heating, Refrigeration and Air Conditioning Engineers (ASHRAE).

ASHRAE have stipulated the criteria for different grades of muffler for different application (Table 1). For application in diesel engines, literature have shown that critical grade is the most suitable grade for muffler design. It was also reported that the diameter of the muffler body should be three times the exhaust pipe diameter d_e [21], [34].

Table 1: ASHRAE standard grades for muffler design [21], [35]

Grade/Parameter	Industrial /Commercial	Residential	Critical	Supercritical
Insertion loss (dBA)	15-25	20-30	25-35	35-40
Body diameter of muffler: exhaust pipe	2-2.5	2-2.5	3	3
Length of muffler: exhaust pipe	5-6.5	6-10	8-10	10-16

Therefore,

$$d = 3 \times de; \quad de = \frac{\mathrm{d}}{3} = 69.3 \text{ mm} \tag{4}$$

where de is exhaust pipe diameter and d is the muffler body diameter.

The mufflers' parameters

Parameters of the mufflers are given in Tables 2.

Table 2: Parameter of muffler samples

Parameters	Sample A (mm)	Sample B (mm)	Sample C (mm)
Shell Diameter	208	208	208
Shell length	800	800	800
First Chamber Length	250	250	250
Second Chamber Length	300	300	300
Third Chamber Length	250	250	250
Outlet diameter	69.3	69.3	69.3
Inlet pipe length	150	150	150
Outlet pipe length	150	150	150
Number of holes on baffle	7	13	26
Diameter of holes on baffle	50	37.5	25
% of total perforated area per plate	40.4	42.5	37.8

Materials Selection

The material selected for this study is stainless steel. Stainless Steel was selected due to its superior corrosion resistance, durability and heat resistance. Air was selected as the working fluid; exhaust gas [23]. The thermo-physical properties of stainless steel as stated by Umair *et al.* are presented in Table 3 [36].

Table 3: Thermo-physical properties of stainless steel

Items	Values
Density	$770\ \mathrm{kg/m^3}$
Specific heat	$420\ \mathrm{J.kg/k}$
Thermal conductivity	$11.2\ \mathrm{W/m.K}$
Thickness	3 mm

Also, the required thermo-physical property of air as reported by [37][38] is as shown in Table 4.

Table 4: Thermo-physical properties of air

Items	Values
Density	$1.225\ \mathrm{kg/m^3}$
Viscosity	$1.7894\ e^{-5}$ kg/m.s

Flow in a duct

The characteristic and the nature of flow in a duct is governed by Reynolds number (*Re*). The *Re* depends on geometry, surface roughness, free stream velocity, surface temperature and types of fluid. It is the ratio of the inertia

force to the viscous force in the fluid [39]. The Reynolds number is as given in Equation (5).

$$Re = \frac{Inertial force}{Viscous force} = \rho \cup \frac{D}{\mu} \; ; \cup = \frac{\mu \times Re}{\rho \times D} \tag{5}$$

For a turbulent flow of *Re* = 20000 and from Equation (5) and Tables 3 and 4, the inlet velocity is calculated to be 4.2157 m/s.

Governing equations

According to Ibrahim [40], the fundamental equations of continuity, momentum and energy transport were adopted for the solution of the problem.

Continuity equation

$$\frac{\partial U_r}{\partial r} + \frac{1}{r}\frac{\partial U_\emptyset}{\partial \emptyset} + \frac{\partial U_x}{\partial x} = 0 \tag{6}$$

U_x is the only non-zero velocity component, thus;

$$U_r = U_\emptyset = 0 \tag{7}$$

Therefore, Equation (6) reduces to:

$$\frac{\partial U_x}{\partial x} = 0 \tag{8}$$

Equation (8) confirms that U_x does not depend on the radial component of the tube which implies a thinned wall tube and also $U_x = U_x(r)$ is the same for all values of x.

$$U_x = U_x(r) \tag{9}$$

Momentum equation

Radial direction:

$$\rho\left(\frac{\partial U_r}{\partial t} + U_r\frac{\partial U_r}{\partial r} + \frac{U_\emptyset}{r}\frac{\partial U_r}{\partial \emptyset} + U_x\frac{\partial U_r}{\partial x} + \frac{{U_\emptyset}^2}{r}\right) = \rho g_r - \frac{\partial P}{\partial r} + \mu\left[\frac{\partial^2 U_r}{\partial r^2} + \frac{1}{r^2}\frac{\partial^2 U_r}{\partial \emptyset^2} + \frac{\partial^2 U_r}{\partial x^2} + \frac{1}{r}\frac{\partial U_r}{\partial r} - \frac{2}{r^2}\frac{\partial U_\emptyset}{\partial \emptyset} - \frac{U_r}{r^2}\right] \tag{10a}$$

Azimuthal direction:

$$\rho\left(\frac{\partial U_\emptyset}{\partial t}+\ U_r\frac{\partial U_\emptyset}{\partial r}+\frac{U_\emptyset}{r}\frac{\partial U_\emptyset}{\partial \emptyset}\ +\ U_x\frac{\partial U_\emptyset}{\partial x}+\frac{{U_\emptyset}^2}{r}\right)=\rho g_\emptyset-\frac{\partial P}{\partial \emptyset}+\mu\left[\frac{\partial^2 U_\emptyset}{\partial r^2}+\frac{1}{r^2}\frac{\partial^2 U_\emptyset}{\partial \emptyset^2}+\frac{\partial^2 U_\emptyset}{\partial x^2}+\frac{1}{r}\frac{\partial U_\emptyset}{\partial r}+\frac{2}{r^2}\frac{\partial U_r}{\partial \emptyset}-\frac{U_\emptyset}{r^2}\right] \quad (10b)$$

Axial direction:

$$\rho\left(\frac{\partial U_x}{\partial t}+\ U_r\frac{\partial U_x}{\partial r}+\frac{U_\emptyset}{r}\frac{\partial U_x}{\partial \emptyset}\ +\ U_x\frac{\partial U_x}{\partial x}\right)=\rho g_x-\frac{\partial P}{\partial x}+\mu\left[\frac{\partial^2 U_x}{\partial r^2}+\frac{1}{r^2}\frac{\partial^2 U_x}{\partial \emptyset^2}+\frac{\partial^2 U_x}{\partial x^2}+\frac{1}{r}\frac{\partial U_x}{\partial r}\right] \quad (10c)$$

Substituting Equations (8) and (9) into Equations (10a) and (10b) in the absence of body force, yields:

$$\frac{\partial P}{\partial r}=0;\frac{\partial P}{\partial \emptyset}=0 \quad (11)$$

Equation (11) shows that pressure depend only on axial direction. Substituting Equations (8) and (9) into Equation (10c) and imposing steady state condition that is:

$$\frac{\partial U_x}{\partial t}=0, \text{ yields;} \quad (12)$$

$$0=\rho g_x-\frac{\partial P}{\partial x}+\mu\left[\frac{\partial^2 U_x}{\partial r^2}+\frac{1}{r^2}\frac{\partial^2 U_x}{\partial \emptyset^2}+\frac{\partial^2 U_x}{\partial x^2}+\frac{1}{r}\frac{\partial U_x}{\partial r}\right] \quad (13)$$

Rearranging Equation (13) gives:

$$\frac{\partial P}{\partial x}=\rho g_x+\mu\left[\frac{\partial^2 U_x}{\partial r^2}+\frac{1}{r^2}\frac{\partial^2 U_x}{\partial \emptyset^2}+\frac{\partial^2 U_x}{\partial x^2}+\frac{1}{r}\frac{\partial U_x}{\partial r}\right] \quad (14)$$

Equation (14) is the momentum transport equation for the models.

Energy equation

The energy transport equation for a steady fluid flow as given:

$$k\frac{\partial^2 T}{\partial r^2}+\frac{k}{r^2}\frac{\partial^2 T}{\partial \emptyset^2}+\frac{\partial^2 T}{\partial x^2}+\frac{k}{r}\frac{\partial T}{\partial r}+\emptyset_{(i)}=\rho C_p\left[U_r\frac{\partial T}{\partial r}+U_\emptyset\frac{\partial T}{\partial \emptyset}+U_x\frac{\partial T}{\partial x}\right] \quad (15)$$

Putting Equation (8) disappears the viscous dissipation term $\emptyset_{(i)}$ and the Equation reduces to:

$$k\frac{\partial^2 T}{\partial r^2}+\frac{k}{r^2}\frac{\partial^2 T}{\partial \emptyset^2}+\frac{\partial^2 T}{\partial x^2}+\frac{k}{r}\frac{\partial T}{\partial r}=\rho C_p\left[U_r\frac{\partial T}{\partial r}+U_{\emptyset}\frac{\partial T}{\partial \emptyset}+U_x\frac{\partial T}{\partial x}\right] \quad (16)$$

Dividing through by k:

$$\frac{\partial^2 T}{\partial x^2}+\frac{1}{r}\frac{\partial T}{\partial r}=\frac{\rho C_p}{k}\left[U_x\frac{\partial T}{\partial x}\right] \quad (17)$$

with:

$$\alpha=\frac{k}{\rho C_p} \quad (18)$$

Equation (17) reduces to:

$$\frac{\partial^2 T}{\partial x^2}=\frac{U_x}{\alpha}\frac{\partial T}{\partial x} \quad (19)$$

Equation (17) is the energy transport equation for flow within the tube.

Mesh convergence test

This is a numerical test required to ensure that the result of the finite element analysis is not affected by changing the size of the mesh. If two subsequent meshing do not change the result substantially, then the mesh has converged which means a stable solution was obtained. Accuracy of Computational Fluid Dynamic depends on mesh convergence and sample geometry which should not be overlooked. For this research 2,988,628 mesh density and 1.8301×10^{-5} (m) mesh size was used. The mesh the convergence graph is shown in Figure 2.

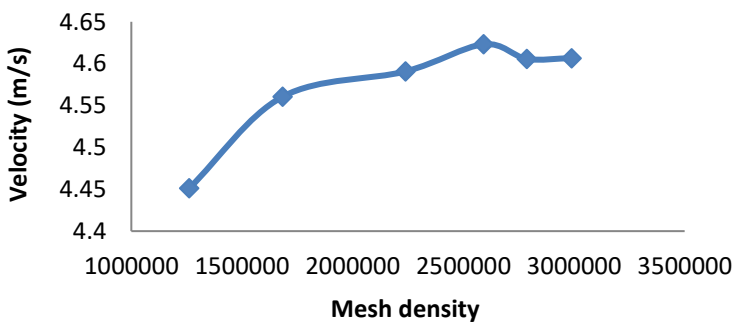

Figure 2: Mesh convergence graph.

Convergence criteria:

The momentum and continuity equations are given in Equation (20) while that of energy transport is in Equation (21). Equations (20) and (21) are the input

parameters into the software for the generation of the data used for the convergence graph.

$$\frac{\emptyset_{1+i}-\emptyset_1}{\emptyset_1} \leq 10^{-5} \quad (20)$$

$$\frac{T_{1+i}-T_1}{T_1} \leq 10^{-6} \quad (21)$$

CFD analysis of the geometries

i. The numerical techniques require three steps, namely; pre-processing which include model drawing, meshing and entering the boundary conditions. Processing involves solving all the governing equations through iteration and post-processing entails accurate analysis of the results [39]. The mufflers were imported into ANSYS 16.0 workbench for numerical simulation. After named selection for each section of the mufflers, the body was meshed both surface and volume meshing on which the accuracy of CFD results depends on and hence the following setups were executed:
ii. The pressure-based solver was used for incompressible flow;
iii. Appropriate physical model: standard K-epsilon and enhance wall treatment was used for accurate turbulent flow only;
iv. Material selection: properties of stainless steel and air were entered.
v. Boundary conditions: the velocity, outlet pressure and constant heat flux were imposed on inlet, outlet and walls;
vi. Solution method: the SIMPLE scheme is used for pressure-velocity coupling and Second Order Upwind for momentum and energy equations are selected under the spatial discretization which is more accurate than First Order especially on unstructured mesh;
vii. Convergence criteria: continuity, X, Y and Z coordinate was set at 10^{-5} and 10^{-6} for energy residual;
viii. Before running the calculation, number of iteration was set at 3000 for solution to converge;
ix. Results: lines were created on the geometries as plane of interest where the velocity, pressure and temperature were evaluated on points along the lines. The velocity contour, velocity vector, pressure contour and temperature contour were generated.

Boundary conditions

The following boundary conditions were applied to obtain solution for continuity, momentum and energy transport equations in numerical simulation of mufflers:

i. The flow was assumed to be steady, non-uniform and incompressible;
ii. The required thermo-physical properties of air were used as an exhaust gas;

iii. Wall was assumed to be stationary wall and therefore, no slip boundary condition was applied;
iv. For reasonably accurate results, realizable K-epsilon model was used for turbulent flow [29], [41], [42];
v. Inlet temperature was 1000 K;
vi. Outlet temperature was 314 K;
vii. Reynolds number was assumed to be 20000 and Inlet velocity was 4.2157 m/s;
viii. Outlet pressure was assumed to be the exit pressure;
ix. Thermal boundary condition of uniform heat flux was applied;
x. Gravity effect was neglected;
xi. The velocity along axial direction was significant while radial and azimuthal were neglected;
xii. Numerical solver was pressure based;
xiii. Convergence criteria for continuity, X, Y and Z coordinate was set at 10^{-5} and 10^{-6} for energy residual;
xiv. Solution method was by simple scheme and second order upwind.

After the application of these boundary conditions, the ANSYS 16.0 was run and the results were generated.

Results validation

Table 5 shows the comparison of the current study with literature.

Table 5: Comparison of the current study with literature

Samples	Inlet velocity (m/s)	Outlet velocity (m/s)	Inlet diameter (mm)	Pressure drop (%)	No. of holes on first baffle	No. of holes on second baffle	Total no. of holes	References
A	19.00	13.10	22.00	2.35	3.	1	4	[36]
B	1.859	1.896	16.66	61.30	3	2	5	
C	1.858	1.917	16.66	67.03	3	2	5	[43]
D*	1.856	1.997	16.66	72.75	3	2	5	
E	4.216	5.551	50.00	85.50	7	7	14	Current
F*	4.216	5.528	37.50	86.70	13	13	26	study
G	4.216	5.505	25.00	85.10	26	26	52	

*Sample with optimum characteristics

It could be observed from the table that as the total number of holes on the baffle increases, the percentage pressure drop also increases. This trend

was observed both in the previous and current studies [36], [43]. Analysis of the results of the current study revealed that back pressure decreases as the diameter of the holes on the baffle and percentage perforated areas increase. This was in agreement with the report of Pangavhane *et al*. and, Teja and Redd [44], [27]. Guhan *et al*. downsize an existing muffler by increasing the number of holes on the inlet pipe from 49 to 70. They reported a significant drop in the back pressure. Studies have shown that the back pressure can be optimized by sizing of baffle holes as well as the number of holes on the baffle and inlet pipe [45],[42]. Therefore, Samples D and F present the optimum performance characteristics from literature and current study, respectively.

Results and discussion

This section contained the results that was obtained from the study as well as discussion of those results**.**

Characteristics of muffler sample A

Figure 3a shows the velocity streamline of the fluid flow in Sample A with inlet and outlet velocities of 4.2157 m/s and 5.5505 m/s, respectively.

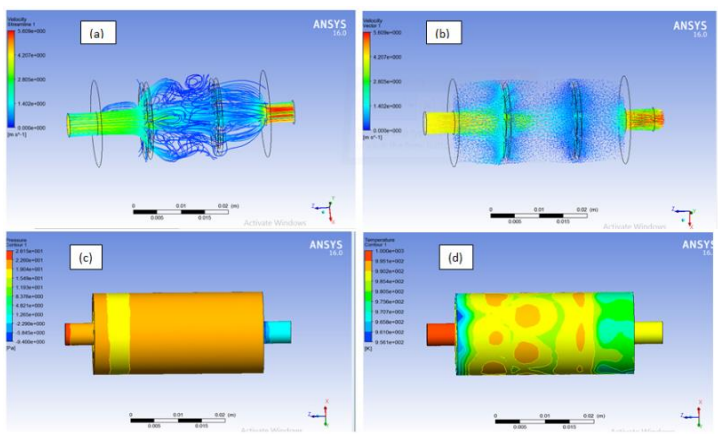

Figure 3: Velocity streamlines, velocity vector, pressure profile and temperature profile of Muffler sample A are shown in (a), (b), (c) and (d), respectively.

The geometry of the inlet and outlet of the sample looks like that of diffuser and nozzle, respectively, which bring about to a decrease in the flow area; increase in pressure and decreases in the velocity of the fluid flow [46]. The high velocity values at the outlet create a low pressure area within the

muffler, hence, lower the pressure buildup. The velocity vector as shown in Figure 3b was very high at the outlet than the inlet of the pipe and likewise high in the first baffle than the second baffle. This is as a result of the obstruction in the flow area. Figure 3c shows that the pressure distribution across the wall of muffler is uniform except at the inlet, first baffle and outlet. The inlet and outlet pressure was 22.2569 Pa and 3.2381 Pa, respectively. Figure 3d shows the temperature profile within the muffler. The temperature decreases along the muffler as a result of heat energy transferred to the environment. The inlet, outlet and average temperatures are 1000, 992.58 and 993.307 K, respectively.

Characteristics of muffler sample B

Figure 4a shows the velocity streamline of fluid flow of sample B. The outlet and inlet velocities are 5.52849 m/s and 4.2157 m/s while the maximum and average velocities of the exhaust gases 6.43036 m/s and 0.873742 m/s, respectively.

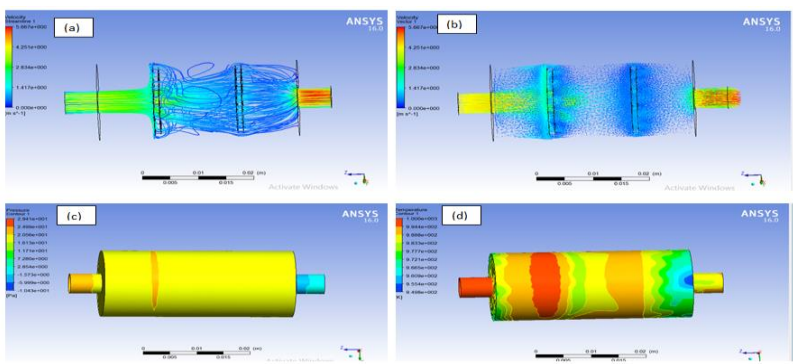

Figure 4: Velocity streamlines, velocity vector, pressure profile and temperature profile of Muffler sample B are shown in (a), (b), (c) and (d), respectively.

Characteristics of muffler sample C

The velocity streamline of fluid flow of Model C is shown in Figure 5a with inlet and outlet velocities of 4.2157 m/s and 5.5047 m/s, respectively and the inlet. The muffler had the maximum and average velocities of 6.79709 m/s and 0.806948 m/s, respectively (Figure 5b). The high velocity at the outlet creates a low pressure within the muffler. Therefore, reduces the pressure buildup in the muffler [27]. Figure 5c displays the pressure distribution was uniform across the wall of muffler except the inlet and outlet pipe, with inlet pressure of 22.4489 Pa and outlet pressure of 3.1994 Pa. Figure 5d shows the temperature profile within the muffler. The inlet temperature was 1000 K

which decreases along the muffler as a result of heat energy transferred to the environment and exhaust gas escaped at the outlet with average temperature of 994.099 K and 995.054 K respectively.

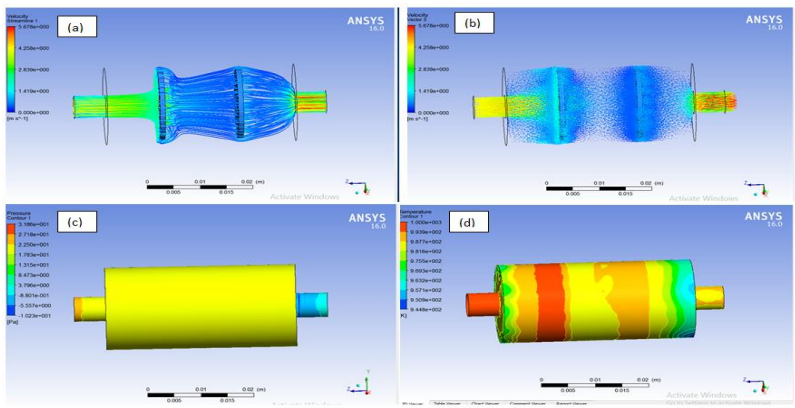

Figure 5: Velocity streamlines, velocity vector, pressure profile and temperature profile of Muffler Sample C are shown in (a), (b), (c) and (d), respectively.

Comparison of mufflers' results

The result of the mufflers were compared in this section.

Pressure contour

Figure 6 shows the variation of flow pressure with axial position along the centerline of the domain. The pressure gradient in the pipe causes the flow to occur in the outlet direction. The three samples have a very close pressure value at the inlet which decreases as it enters the first chamber. There was sudden increase in pressure of sample C at the first baffle with the highest backpressure and lowest pressure reduction while sample A with the lowest backpressure. At the inlet of the outlet pipe, there is a rapid pressure drop as the gas exits the muffler and the pressure was independent on the number of holes on the baffle at axial positions 0 - 300 mm. It was observed that pressure was almost constant between the baffles to the third chamber for the entire sample consider. This was in agreement with the work of Pangavhane *et al. and* Chaudhri *et al*. They reported that backpressure decreases as the diameter of holes increases on the pipe [47], [28]. Therefore, sample A will perform better than samples B and C.

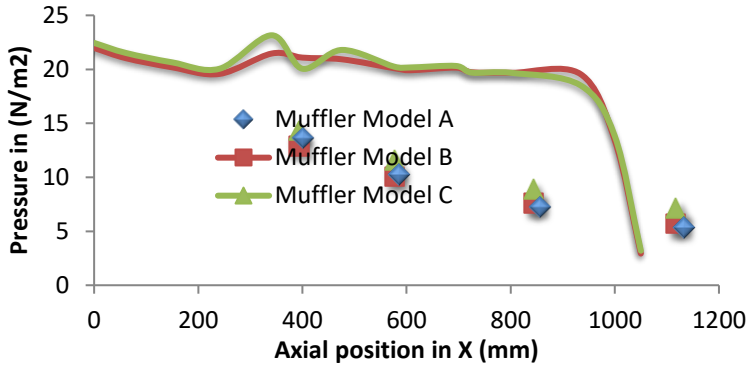

Figure 6: Variation of flow pressure with axial position along the centerline of the domain 4.

Velocity contour

Figure 7 shows the variation of flow velocity with axial position along the centerline of the domain. The lowest and highest velocity was observed with samples A and B, respectively. The results show a close velocity value at the inlet of the pipe and increases on entering the first chamber. There was a drop in the velocity at the first baffle and further attenuate between the baffles. The exit velocities of samples A, B and C are 5.13785, 5.0971 and 5.085 m/s, respectively. Analysis of the results shows that the velocity of flow is independent of the number of holes on the baffle at axial positions 0 mm to 300 mm and greater than 1000 mm. This explains the reason why sample A had the lowest pressure at the outlet pipe which was because of its higher velocity compare with other samples. The main factor behind good scavenging is exit velocity. The fast moving pulse creates a low pressure area behind, hence, muffler sample A will experience lowest pressure buildup than B and C [27].

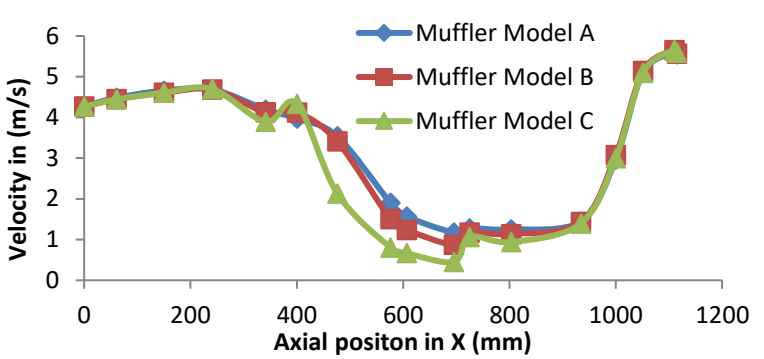

Figure 7: Variation of flow velocity with axial position along the centerline of the domain.

Temperature contour

Figure 8 shows the variation of flow temperature with axial position along the centerline of the domain. It was observed that the temperature of models reduces from the inlet to the outlet pipe of the as the fluid travel in the pipe and this was due to temperature gradient. The temperature of the inlet was the same for all samples. Results shows that temperature in the pipe depends on the number of holes at axial position greater than 300 mm. Sample A was having the lowest outlet and average wall temperature because it retains less hot exhaust gas compared to other samples. This shows that sample A would have more resistance to thermal crack and leakages than samples. This is because high temperature can badly affect the microstructure of ferrous alloy which can cause thermal degradation, cracking, leakage and exposure to corrosion [27]. The characteristics of muffler samples are shown in Table 6.

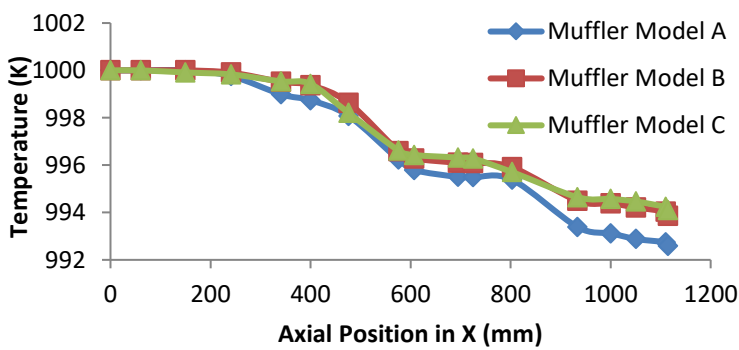

Figure 8: Variation of flow temperature with axial position along the centerline of the domain.

For a muffler to function effectively in term of fuel efficiency and durability, it must have low back pressure, low forces on the walls and baffles [28]-[27]. Considering these parameters, Table 7 shows parameters combination for the muffler samples and the percentage was based on each optimal parameter achieved in the muffler.

Table 6: The obtained characteristics of muffler samples

Parameters	Muffler Sample A	Muffler Sample B	Muffler Sample C
Inlet Pressure (Pa)	22.2569	21.9802	22.4489
Outlet Pressure (Pa)	3.2381	2.93326	3.1994
Back Pressure (Pa)	20.2352	21.4626	23.1539
Pressure Reduction (Pa)	85.5%	86.7%	85.1%
Diameters (mm)	50	37.5	25
Numbers of Holes	7	13	26
Perforated Area(mm^2)	13,746	14,360	12,764
% Perforated Area(mm^2)	40.4	42.5	37.8
Average Flow Rate ($x10^{-2}$ m^2/s)	1.2158	1.2547	1.0299
Average Wall Temperature (K)	986.311	988.35	988.457
Average Wall Shear	0.092590	0.088137	0.0890299
Volumetric Flow Rate ($x10^{-3}m^3/s$)	12.16	12.55	10.29
Turbulence Eddy Dissipation(m^2/s^3)	122.287	126.79	153.476
Force on Baffle One ($x10^{-7}N$)	4.75429	1.4549	1.5772
Force on Baffle Two ($x10^{-8}N$)	4.3754	1.31129	5.007
Force on the Body Walls ($x10^{-6}N$)	4.0018	3.16198	5.09015

Table 7: Parameters combination for muffler A, B and C

Parameters (%)	Muffler A	Muffler B	Muffler C
Backpressure	87.4	92.7	100
Wall Shear	100	95	96
Force on Baffle 1	100	30.6	33.2
Force on Baffler 2	87.4	26.0	100
Force on the Wall	79	62	100
Average wall Temperature	99	100	100

Conclusion

Numerical investigation on mufflers was carried out on three different mufflers using the governing equations that guide the fluid flow and muffler design. Analysis of the results shows that muffler sample A with 50 mm diameter and 40.4% perforated area had the lowest backpressure 20.2352 Pa and average wall temperature 986.311 K which is desirable for engine optimum engine

performance and fuel efficiency. Muffler B with 37.5 mm diameter and 42.5 % perforated area has the lowest forces on the muffler is also important for muffler durability and muffler C has the least advantage when compared with other samples. The average flow rate and volumetric flow rate increase with increase in the percentage perforated areas. Outlet and maximum velocities decreases with increase in the number of holes on the muffler while the average and outlet temperatures increase with increase in the number holes on the muffler. It could be concluded that muffler sample B had the optimum performance characteristics for design purpose particularly when considering fuel consumption, engine efficiency and muffler durability.

References

[1] S. V Mahesh and P. V Jotaniya, "A Review of Heat Transfer Analysis in Automotive Exhaust System," *Int. J. Innov. Res. Sci. Eng. Technol.*, vol. 4, no. 2, pp. 558–561, 2015.

[2] X. Zhu and Ö. Andersson, "Performance of new and aged injectors with and without fuel additives in a light duty diesel engine," *Transp. Eng.*, vol. 1, pp. 1–9, 2020.

[3] S. Misaghi, C. Tirado, S. Nazarian, and C. Carrasco, "Impact of pavement roughness and suspension systems on vehicle dynamic loads on flexible pavements," *Transp. Eng.*, vol. 3, pp. 1–9, 2021.

[4] G. D. Rubio, R. L. P. Teixeria, R. A. M. Carrillo, V. T. Signoretti, V. C. DepLacerda, and R. F. Brito, "Numerical Analysis of the Thermal and Aerodynamic Influence in an Automotive Exhaust System Using Computational Fluid Dynamic," *Am. J. Eng. Res.*, vol. 6, no. 2, pp. 20-27, 2017.

[5] P. Xu, H. Jiang, and X. Zhao, "Analysis of Flow Field and Pressure Loss for Fork Truck Muffler Based on The Finite Volume Method," *Int. J. Heat Technol.*, vol. 33, no. 3, pp. 85–90, 2015.

[6] J. Xu and Z. Shusting, "Analysis of Flow for Automotive Exhaust System Based on Computational Fluid Dynamic (CFD)," *Open Mech. Eng. J.*, vol. 8, pp. 587–593, 2014.

[7] M. Herrmann, R. Jöst, F. Kehl, A. Özkan, S. Pless, and F. Gauterin, "Importance of Vehicle Body Elements and Rear Axle Elements for Describing Road Booming Noise," *Vehicle*, vol. 2, pp. 589–602, 2020.

[8] P. Xu, H. Jiang, and X. Zhao, "CFD Analysis of Gasoline Engine Exhaust Pipe," *J. Appl. Mech. Eng.*, vol.17, no. 2, pp.7.1-7.5, 2016.

[9] S. Wang, G. Shi, and Y. Lin, "Integrated hierarchical control strategy of active suspension and differential assisted steering system for electric-wheel vehicle," vol. 81, no.3-4, pp. 212–240, 2019.

[10] C. E. Okafor, O. O. Oghenemaero, M. Chukwuebuka, and O. O. Isaac, "Adaptive design of a universal automotive ball joint separating device,"

Transp. Eng., vol. 2, no. April, pp. 1–12, 2020.
[11] P. Neri, F. Bucchi, and D. Passarelli, "A multilevel finite element-multibody approach to design the suspension system for the road transportation of SSR1 cryomodule," *Transp. Eng.*, vol. 2, pp. 1–9, 2020.
[12] J. Wangie and P. V. Dong, "The Model Analysis of Automotive Exhaust Muffler Based on PRO/E and Ansys," *3rd Int. Conf. Adv. Comput. Theory Eng.*, 2010.
[13] D. P. Snezana, B. P. Radiovoje, and K. Lukic, "Heat Transfer in Exhaust System of A Cold Start Engine at Low Environmental Temperature," *Therm. Sci.*, vol. 4, pp. 209–220.
[14] O. Ariara, C. P. Guhan, G. Arthanareeswaren, and K. N. Varadarajan, "CFD Study on Pressure Drop and Uniformity Index of Three Cylinder LCV Exhaust System," *Procedia Eng.*, vol. 127, pp. 1211–1218, 2015.
[15] B. Mohamad, J. Karoly, A. Zelentsov, and S. Amroune, "A hybrid method technique for design and optimization of Formula race car exhaust muf fl er," *Int. Rev. Appl. Sci. Eng.*, vol. 5, no. 2, pp. 174–180, 2020.
[16] U. Mohd, A. P. AbdulBasit, and G. Anshul, "Modification in Muffler Design to Reduce the Back Pressure," *Int. J. Innov. Res. Sci. Eng. Technol.*, vol. 5, pp. 8045–8052, 2016.
[17] J. K. Lee, K. S. Oh, and J. W. Lee, "Methods for evaluating in-duct noise attenuation performance in a muf fl er design problem," *J. Sound Vib.*, vol. 464, pp. 114982, 2020.
[18] C. H. G. Brito, C. B. Maia, and J. R. Sodre, "A Mathematical Model for the Exhaust Gas Temperature," *4th Int. Conf. Math. Model. Phys. Sci. J. Phys. Conf. Ser.*, vol. 688, 2015.
[19] S. Peter, C. P. L. Mirko, and P. Jurij, "A Muffler with Adaptive Acoustic Properties," *J. Mech. Eng.*, vol. 61, pp. 553 – 560, 2015.
[20] K. R. Gadre and T. A. Jadhav, "Vibration Analysis of an Automotive Silencer," *Int. J. Innov. Eng. Res. Technol.*, vol. 2, no. 6, pp. 1–7, 2015.
[21] Y. K. Kakadiya, B. S. Patel, and J. P. Hadiya, "Design and Comparison of Mufflers Having Different Arrangement for Diesel Engine," *SSRG Int. J. Mech. Eng.*, vol. 4, no. 3, pp. 123–131, 2017.
[22] P. V Lokhande and N. Arum, "Design Development and Analysis of Reactive Type Resonator Chamber Muffler for Internal Combustion Engine: A Review," *Int. J. Sci. Res. Dev.*, vol. 4, no. 1, pp. 615–618, 2016.
[23] S. Kore, A. AbdulKadir, and D. Eddesa, "Performance Evaluation of a Reactive Muffler Using CFD," *J. EEA*, vol. 28, 2011.
[24] A. Elsayed, C. Bastien, S. Jones, J. Christensen, H. Medina, and H. Kassem, "Case Studies in Thermal Engineering Investigation of baffle con fi guration effect on the performance of exhaust mufflers," *Case Stud. Therm. Eng.*, vol. 10, pp. 86–94, 2017.
[25] B. Chandrashekhar, S. S. Sharma, K. Jagannath, N. S. Moham, and S. G. Sathisha, "Design and Analysis of Expansion Chamber Muffler," *World J. Eng.*, vol. 7, no. 3, pp. 117–118, 2010.

[26] A. S. Mate and V. Kumbhar, "Thermal Analysis of Silencer Pipe," *Int. J. Mech. Eng. Technol.*, vol. 8, no. 3, pp. 269–279, 2017.

[27] P. S. R. A. Teja and K. H. C. Reddy, "Backpressure Study in Exhaust Muffler of Single Cylinder Diesel Engine using CFD Analysis," *Int. J. Creat. Res. Thoughts*, vol. 6, no. 2, pp. 335–344, 2018.

[28] J. H. Chaudhri, P. B. S. Patel, and P. S. A. Shah, "Muffler Design for Automotive Exhaust Noise Attenuation - A Review," *Int. J. Eng. Res. Appl.*, vol. 4, no. 1, pp. 220–223, 2014.

[29] R. G. Ramganesh and J. Devarad, "Simulation of Flow And Prediction of Back Pressure of the Silencer Using CFD," *J. Chem. Pharm. Sci. "Natural Conf. Recent Trends Dev. Sustain. Green Technol.*, SI 7, pp. 297 – 300, 2015.

[30] N. Safaei, C. Zhou, B. Safaei, and A. Masoud, "Gasoline prices and their relationship to the number of fatal crashes on," *Transp. Eng.*, vol. 4, pp. 1–10, 2021.

[31] C. C. Krunal, R. Y. Patil, N. R. Suryawanshi, and S. J. Chaudhari, "Investigation of Geometric Parameter on Performance of Muffler using CFD Analysis," *Int. Res. J. Eng. Technol.*, vol. 3, no. 12, pp. 1332–1338, 2016.

[32] M. D. Nasiruddin, M. M. AhbaburRahman, N. A. N. Rashid, and J. I. Rony, "Reduce Generator Noise with Better Performance of A Diesel Generator Set Using Modified Absorption Silencer," *Glob. J. Res. Eng.*, vol. 16, no. 4, pp. 45–53, 2016.

[33] P. S. Kumar *et al.*, "Design and construction of a reactive type muffler for a formula student vehicle," *Int. J. Mech. Eng. Technol.*, vol. 9, no. 5, pp. 83–93, 2018.

[34] K. C. Chaudhari, R. Y. Patil, N. R. Suryawanshi, and S. J. Chaudhari, "Investigation of Geometrical Parameter on Performance of Muffler Using CFD Analysis," *Int. Res. J. Eng. Technol.*, vol. 3, no. 7, pp. 1332–1338, 2016.

[35] G. G. Reddy and N. Prakash, "Design and Fabrication of Reactive Muffler," *Int. J. Chem. Sci.*, vol. 14, no. 2, pp. 1069–1076, 2016.

[36] M. Umair, A. Basit, A. Prabhakar, and A. Gautam, "Modification in Muffler Design to Reduce the Backpressure," *Int. J. Innov. Res. Sci.*, vol. 5, no. 5, pp. 8045–8052, 2016.

[37] S. M. Trivedi, S. Bansode, and P. Pawar, "CFD Flow Analysis and Optimization of Exhaust," *Int. J. Res. Appl. Sci. Eng. Technol.*, vol. 5, no. 8, pp. 86–91, 2017.

[38] S. E. Abdelghany, O. E. Abdellatif, G. Elhariry, and E. E. Khalil, "*NACA653218airfoil Aerodynamic Properties*," *Institute of Aviation Engineering*, 2019. [Online]. Available: https://www.researchgate.net/publication/305217292_NACA653218_Airfoil_Aerodynamic_Properties. [Accessed: 04-Apr-2021].

[39] Y. A. Cengel and A. J. Ghajar, *"Heat and Mass Transfer Fundamentals*

and Applications," 5th Ed. Grawhil Educ. Stillwater., 2015.
[40] I. B. Ibrahim, "Numerical Simulation of Laminar Flow of A Non-Newtonian Viscous Fluid in a Rhythmical Non–Permeable Medium," *M.Eng Thesis Dep. Mech. Eng. , Fac. Eng. Univ. Ilorin*, 2014.
[41] A. Moen, L. Mauri, and V. D. Narasimhamurthy, "Comparison of k - ε models in gaseous release and dispersion simulations using the CFD code FLACS," *Process Saf. Environ. Prot.*, vol. 130, pp. 306–316, 2019.
[42] C. P. O. A. Guhan, G. Arthanareeswaran, K. N. Varadarajan, and S. Krishnan, "Exhaust System Muffler Volume Optimization of Light Commercial Vehicle Using CFD Simulation," *Mater. Today Proc.*, vol. 5, pp. 8471–8479, 2018.
[43] K. C. Chaudhari and P. S. J. Chaudhari, "Investigation of Structural Parameter of Perforated Muffler for Performance Optimization Using CFD Analysis," *Int. J. Res. Appl. Sci. Eng. Technol.*, vol. 5, no. 10, pp. 2257–2264, 2017.
[44] S. D. Pangavhane, A. B. Ubale, V. A. Tandon, and D. R. Pangavhane, "Experimental and CFD Analysis of a Perforated Inner Pipe Muffler for the Prediction of Backpressure," *Int. J. Eng. Technol.*, vol. 5, no. 5, pp. 3940–3950, 2013.
[45] O. Erdem, Y. Rifat, and P. Zeynap, "An Analysis of Geometric Parameters Effect on Flow Characteristic of a Reactive Muffler," *17th Int. Res. Conf. Trend Dev. Mach. Assoc. Technol. TMT 2013, Istanbul, Turkey*, 2013.
[46] O. A. Osore, "Essentials of Classical Thermodynamics," *Dep. Mech. Eng. Fed. Polytech. Ilaro, Ogun State Niger.*
[47] D. P. Sudarshan, B. U. Amoi, and D. Pangavhane, "Experimental and CFD Analysis of A Perforated Inner Pipe Muffler for the Prediction of Back Pressure," *Int. J. Eng. Technol.*, vol. 5, no. 5, pp. 3940 – 3950, 2013.